HHS Public Access

Author manuscript

Magn Reson Med. Author manuscript; available in PMC 2019 February 01.

Published in final edited form as:

Magn Reson Med. 2018 February ; 79(2): 912–922. doi:10.1002/mrm.26759.

RELATIONSHIP OF CHANGES IN STRAIN RATE INDICES ESTIMATED FROM VELOCITY-ENCODED MR IMAGING TO LOSS OF MUSCLE FORCE FOLLOWING DISUSE ATROPHY

VADIM MALIS[1,2], **USHA SINHA**[3], **ROBERT CSAPO**[1], **MARCO NARICI**[4], and **SHANTANU SINHA**[1]

[1]Muscle Imaging and Modeling Lab, Dept. of Radiology, UC San Diego, San Diego, California, USA

[2]Physics, UC San Diego, San Diego, California, USA

[3]Physics, San Diego State University, California, USA

[4]School of Graduate Entry Medicine and Health University of Nottingham, Derby, UK

Abstract

Purpose—This study explores changes in strain rate (rate of regional deformation) parameters extracted from velocity encoded MRI and their relationship to muscle force loss following 4-week unilateral lower limb suspension (ULLS) in healthy humans.

Methods—2D SR maps were derived from three directional velocity encoded magnetic resonance phase-contrast images of the medial gastrocnemius in seven subjects. Atrophy related and regional differences in the SR eigenvalues, angle between the SR and muscle fiber (SR-fiber angle), and strain rates in the fiber basis were statistically analyzed using ANOVA and linear regression.

Results—During isometric contraction, SR in the fiber cross-section ($SR_{in\text{-}plane}$) was significantly lower and SR-fiber angle was significantly higher post- suspension ($P<0.05$). On multiple variable regression analysis, volume of medial gastrocnemius, $SR_{in\text{-}plane}$, and SR-fiber angle were significantly associated with force and changes in the, SR eigenvalues and shear strain rate were significantly associated with change in force with disuse.

Conclusion—Changes in SR-fiber angle, $SR_{in\text{-}plane}$ and shear strain rate as well as their ability to predict force/force changes may reflect the role of remodeling of the extracellular matrix in disuse atrophy and its functional consequence in reducing lateral transmission of force.

Keywords

Unilateral limb suspension; Chronic atrophy; Velocity encoded MRI; Muscle strain rate tensor; Shear strain rate; lateral transmission of force

Corresponding Author Shantanu Sinha Ph.D., RIL, Dept. of Radiology, UCSD, 3510 Dunhill Street, San Diego, CA-92121, Ph.No.: 858-534-2004, shsinha@ucsd.edu.

INTRODUCTION

It is well established that chronic unloading of muscle results in rapid skeletal muscle atrophy and is accompanied by a significant loss in the capacity to generate force during contraction (1). Atrophy (reduction in myofiber and whole muscle size) is the result of a decrease in protein synthesis and an increase in protein degradation that ultimately leads to a loss of contractile proteins, organelles, nuclei, and cytoplasm (2,3). Narici and Cerretelli used plaster cast induced immobilization in human subjects to create a model of unilateral disuse atrophy (4) and demonstrated that, in disuse atrophy, both fiber length and pennation angle decrease, suggesting a loss of sarcomeres in series and in parallel, respectively. Muscle remodeling (measured by changes in fiber length, pennation angle and muscle thickness) with inactivity is an extremely fast process occurring after even 7–8 days of inactivity (5–7). De Boer et al. employed the Unilateral Limb suspension (ULLS) model to unload the human knee extensors and reported, after 14 days of suspension, a decrease in Focal Adhesion Kinase content (−20%) and activity (−30%), associated with a 50% fall in muscle protein synthesis and a 5% decrease in quadriceps muscle anatomical cross-sectional area (ACSA) (8). A particular noteworthy observation of the above study, as in most unloading studies, is that the decrease in muscle force exceeded that of muscle size, with the loss of quadriceps force after 2 weeks of ULLS being greater than ~3-fold that of muscle ACSA, even after accounting for changes in muscle activation (8). Although some of this phenomenon may be partly explained by a decrease in single fiber specific tension (force per unit ACSA of single fibres) (9,10), recent evidence suggests that changes in the extracellular matrix (ECM) can substantially contribute to this disproportionate loss of force (11). This is because force transmission occurs both longitudinally along the muscle fiber and laterally through the adjacent ECM and muscle fibers to the epimysium of the skeletal muscle (12,13) and impairment of lateral force transmission can account up to 50% of force loss in dystrophic mice and very old rats (14). Several reports based on physiologically based computational models have identified that the mechanism by which force is transmitted laterally is through shear strain in the ECM (15). Measurement of shear strain may thus allow an indirect assessment of lateral transmission of force (LTF).

Velocity encoded magnetic resonance (MR) imaging is a convenient method to map tissue motion in all three directions and Strain Rate (SR) can be directly extracted from the acquired dynamic MR images. Strain is a measure of tissue deformation with respect to a reference state and requires tissue tracking. On the other hand, Strain Rate, i.e. the instantaneous change of strain with time, describes the rate of regional deformation and does not require $3D^{al}$ tracking or a reference state. SR tensor mapping provides important information on both the magnitude and orientation of the rate of deformation. Strain rate is conveniently represented as tensors (the current analysis is performed a 2D image resulting in a 2×2 tensor), where the terms along the diagonals are the normal strain rate magnitudes in two orthogonal directions and the off-diagonal terms are the shear strain rate terms. The normal strain rate measures the amount of deformation parallel to a given line, while the shear strain rate measures the amount of deformation perpendicular to a given line. A positive SR indicates a local expansion while a negative SR indicates a local contraction. A previous study used MR dynamic imaging to investigate age related changes in muscle

mechanical properties and contractility by mapping strain rate tensors derived from velocity encoded images (16). The main findings of the aging study indicated that the mechanical properties of the extracellular matrix have a role in determining the change in strain rate and its spatial patterns in the aging muscle.

The Unilateral Limb Suspension (ULLS) model of atrophy and muscle force loss is another perturbation of the normal muscle that has similarities to aging muscle but important differences as well. While the aging model represents a chronic state, the ULLS model represents a transient state in which muscle function, *ceteris paribus*, will be determined by the timing of loss of contractile tissue together with remodeling of passive structures (connective tissue) within the muscle which undergo important qualitative and quantitative changes. There are known structural and material changes with ULLS induced acute atrophy in muscle (8,17,18); thus indices derived from the SR tensor could potentially be used as surrogate imaging biomarkers of these changes.

The focus of this paper is to explore (i) the changes induced by disuse atrophy in parameters derived from the SR tensor including normal and shear strain rates and (ii) the relationship between the changes in SR parameters to force loss from disuse atrophy. The specific hypothesis was that SR parameters potentially affected by ECM remodeling (SR-fiber angle, shear strain) would be related significantly to force loss in disuse atrophy. The hypothesis was tested on the medial gastrocnemius (MG) during submaximal isometric contraction.

METHODS

Ethical Approval-Subjects—Seven subjects (2 female, 5 male) were included in this study after written informed consent had been obtained (29.1 ± 5.7 year old, body mass 75.4 ± 22.7 kg, height 168.1 ± 7.4 cm). The criterion for inclusion was that subjects should be moderately active. Subjects participating in competitive sports as well as those with any surgical procedures performed on the lower leg were excluded. The study was carried out under the approval of the Medical Research Ethics Board of University of California San Diego and conformed to all standards for the use of human subjects in research as outlined in the Declaration of Helsinki on the use of human subjects in research.

Study design—The effect of chronic unloading and rehabilitation on the force production capability and strain distribution patterns of the MG muscle was assessed by comparing the baseline (Pre) to immediately after 4 week of limb suspension (Post). During the suspension period, subject compliance to the protocol was monitored at 2 weeks to check for loss in force production as well as muscle atrophy (MRI morphological scan). In addition, a wireless activity tracker was integrated into the crutches for independent confirmation of compliance; the subject was not informed of the tracker to ensure that it was not removed or tampered with to simulate crutch usage. After the 4-week suspension, subjects were required to attend physical rehabilitation sessions. A final imaging study at the end of the rehabilitation period (4 weeks) was performed to confirm that the muscle had recovered to baseline status.

Unilateral Limb Suspension (ULLS)—Muscle atrophy was induced on the non-dominant leg with 4 week of chronic unloading using the ULLS model (19), which has been used extensively in many earlier studies. Subjects identified the dominant leg as the one they preferentially used to regain balance from a jostle. The non-dominant leg was the left leg for all subjects in this study. The ULLS protocol allowed the subjects a reasonable amount of freedom to carry out their daily activities as well as driving since the dominant leg (right in this study) was not unloaded. A crutch was used to prevent the foot (of the left leg) from touching the ground. The right foot was raised with a 5-cm heel on the shoe to further minimize accidental loading of the foot.

MR imaging—MR imaging was performed on a 1.5 Tesla Signa HDx MR scanner (GE Medical Systems, Milwaukee, WI), with the subject lying supine, feet first, with the left leg (i.e., the non-dominant leg to be imaged) placed in a cast. An optical fiber pressure transducer was glued to the sole of the cast that was firmly anchored to the radiofrequency coil by means of Velcro straps. Pressure exerted against the cast during isometric contraction was detected by the transducer, converted to a voltage by a spectrometer (Fiberscan, Luna Innovations, Roanoke, VA) and used to trigger the MR image acquisition. For data analysis, the voltage output from the pressure transducer was later converted into units of force (N) based on a calibration of the system using disc weights. Images were acquired during submaximal, isometric contraction at 35% of the individual maximum voluntary contraction (MVC). The MR image acquisition was completed in ~70 cycles; thus it was important to ensure consistency of motion. This was ensured by providing the subject with real-time visual feedback of the actual force generated by the subject superposed on the target force curve to facilitate consistent contractions.

The MR images used in this report include high-resolution water saturated oblique sagittal fast spin echo images of the MG (TE: 12.9 ms, TR: 925 ms, Averages: 4, Flip Angle: 20°, slice thickness/gap: 3/0 mm, Field of View: 30 × 22.5 cm, Matrix: 512 × 384). This sequence provides a high tissue contrast for the fascicles in the background of suppressed muscle signal and was used to locate fascicle end points. The orientation that best depicted the fascicles was selected for the Velocity-Encoded Phase Contrast (VE-PC) scans. Oblique sagittal slices were obtained with the following acquisition parameters: Echo Time: 7.7 ms, Repetition Time: 16.4 ms, Averages: 2, Flip Angle: 20°, slice thickness: 5 mm, Field of View: 30 cm × 22.5 cm (partial phase Field of View: 0.75), 256 × 192 matrix (lower resolution in the phase direction), 4 views/segment, 5–7 slices, 22 phases, 10 $cm{\cdot}s^{-1}$ three directional velocity encoding. This resulted in 72 repetitions [(192 (phase encode) ×2 (averages) ×0.75 (phase FOV))/4 (views/segment) = 72] for each slice acquisition. The temporal resolution is calculated as: 16.4(TR)*4 (views/segment)*4 (velocity encoding directions)/2 (view sharing)= 131 ms (confirmed in the DICOM header). Twenty-two phases were collected within each isometric contraction-relaxation cycle of ~3 s (22*131ms= 2.88s).

Force measurements—Isometric MVC of the plantarflexor muscles was determined for each subject prior to MR imaging. For this purpose, the ankle was fixed in a neutral position (90° angle between the axis of the foot and the shank). The best of three trials was used to

set the target level of force for subsequent image acquisition (35% of MVC). During the subsequent execution of the ~70 contraction-relaxation cycles, torques were recorded at a sampling frequency of 200 Hz and then averaged over repeated cycles to produce curves of mean force.

Morphological Quantification and Normalized Force of the Triceps Surae (TS) muscles—TS force per unit of anatomical cross-sectional area (F/ACSA) was determined as the ratio of plantarflexors MVC to TS ACSA represented by the sum of the maximum ACSA of MG, lateral gastrocnemius (LG) and soleus (SOL). Maximum ACSA was defined as the maximum value of ACSA selected from all the axial images for each muscle. In order to estimate the maximum force acting along the TS tendon, the force recorded by the force transducer was divided by the Achilles tendon moment arm corresponding to 90° angle between the axis of the foot and the shank detailed earlier (20). In brief, a sagittal MR image of the lower leg and foot was used to identify the joint (ankle) center of rotation as well as Achilles tendon line of action (the latter marked as a straight line along the center of the tendon). The perpendicular distance of the joint center to the line of action was measured as the Achilles tendon moment arm (21). Physiological Cross Sectional Area (PCSA) of the MG was computed as the ratio of the volume of the MG to the average fiber lengths. Fiber lengths were computed by identifying fascicles in the MG seen in the fast spin echo images (See section on Muscle fiber tracking) in the mid-MG region.

Image Analysis

Strain rate (SR) Calculation—Phase images were corrected for phase shading artifacts and denoised with an anisotropic diffusion filter. The SR tensor was calculated in the following steps by: (i) computing the tensor L, from the derivative of the velocity images: given that u and v represent the x- and y components of the velocity vector with respect to the x- and y- axis.

$$L=\begin{bmatrix} \partial u/\partial x & \partial u/\partial y \\ \partial v/\partial x & \partial v/\partial y \end{bmatrix} \quad [1]$$

(ii) The symmetric part of the SR tensor was then calculated as: $0.5(L+L^T)$. The SR tensor was then diagonalized to obtain the eigenvalues and eigenvectors. The values were sorted as positive and negative values at each voxel (in s^{-1} scaled by 1000) and with their corresponding eigenvectors, stored as separate images. Deformation of tissues within the muscle can be represented along 3 principal SR directions: SR_{fiber}, $SR_{in\text{-}plane}$ and $SR_{through\text{-}plane}$. SR_{fiber} denotes deformation approximately along the muscle fiber long axis that is negative (NEV) during muscle fiber shortening (phases 1–11) and positive (PEV) during relaxation (phases 12–22). It is important to note that it is the presence of shear forces that causes the axis of SR_{fiber} to be rotated away from the muscle fiber long axis; this angle is referred to as the SR-fiber angle (see section *Muscle fiber tracking*). $SR_{in\text{-}plane}$ by contrast, is defined as deformation in a direction approximately orthogonal to that and in the imaging plane and is characterized by eigenvalues with a sign opposite to that of SR_{fiber}.

$SR_{through\text{-}plane}$, which is the SR in the fiber cross-section perpendicular to the imaging plane (i.e., the plane of the muscle fibers) was derived from the SR measured in the other two directions. It is computed based on the assumption of volume incompressibility of muscle tissue: a local longitudinal contraction along the muscle will be accompanied by a local radial expansion in the plane perpendicular to the fiber. It is fairly well accepted that muscle, because of its high fluid content, is incompressible (22,23). For a 3D volume that is incompressible, the sum of the three strain rates should be zero. Here, only the 2D tensor can be calculated, so the sum of the two measured eigenvalues was used to infer the magnitude of the third eigenvalue as:

$$\mathrm{SR}_{\mathrm{through-plane}} = -(\mathrm{SR}_{\mathrm{fiber}} + \mathrm{SR}_{\mathrm{in-plane}}) \quad [2]$$

The deformation in the fiber cross-section can range from symmetric, moderately and severely asymmetric with greater deformation in-plane and moderately and severely asymmetric with greater deformation through-plane; a schematic is shown in (16).

Muscle fiber tracking—In the absence of shear forces, the principal SR directions would be strictly determined by the orientation of muscle fibers (i.e. the principal axis of contraction will be parallel to the muscle fiber orientation). However, SR_{fiber} is typically rotated away from the fiber long axis, that is, in addition to normal deformation, there is also shear deformation, requiring the principal strains to be related to the coordinate system represented by muscle fibers. To determine this coordinate system, the origin and insertion points of muscle fibers were identified at seven locations along the muscle length on the sagittal-plane fast spin-echo images and transferred to the first frame of the dynamic images. Briefly, the origin and insertion points of the muscle were identified on water suppressed sagittal images in which the fascicles appeared with high contrast against a background of dark muscle tissue (24). The oblique sagittal images were acquired so that the muscle fibers (and fascicles) lay in the imaging plane. A muscle physiologist (RC) identified the fascicle end points on the deep and superficial aponeurosis. A line connecting these end points provided a good approximation to a muscle fiber. The initial identification of the fascicles was corrected on the magnitude images of the VE-PC since small mismatches in image geometry were found between the fast spin-echo and the VE-PC images. The VE-PC cines were used to track the coordinates of these points across the contraction-relaxation cycles. Muscle fiber orientation with respect to the positive x-axis was calculated at each phase of the dynamic cycle. The seven locations were grouped into three groups (2 distal, 3 middle, 2 proximal) and averaged to represent the typical MG behavior in these regions. The angle subtended by SR_{fiber} and the muscle fiber direction was determined and is referred to, in the rest of the paper, as the SR-fiber angle.

Strain in the fiber basis—To quantitate shear strains, the SR in the principal axis needs to be projected onto the muscle fiber, which is accomplished by rotating the SR tensor to the fiber basis. Consider the 2D configuration of the SR eigenvalues and fiber shown in the schematic (Figure 1), where f is the fiber direction, c is the fiber in-plane cross-section direction, NEV and PEV are the negative and positive principal strains respectively and θ is

the SR-fiber angle. In order to obtain the strain tensor in the fiber/cross-section basis ($SR_{fiber\text{-}basis(fb)}$), the SR tensor in the principal axis frame is rotated by θ to obtain:

$$SR_{fb}=\begin{pmatrix} SR_{cc} & SR_{cf} \\ SR_{fc} & SR_{ff} \end{pmatrix} \quad [3]$$

where SR_{ff} is the normal strain along the fiber, SR_{cc} is the normal strain in the fiber cross-section, and SR_{fc} (= SR_{cf}) is the shear strain. In the fiber basis, the shear strain, SR_{fc} is given by:

$$SR_{fc}=\frac{PEV-NEV}{2}\sin 2\theta \quad [4]$$

Figure 1b illustrates the origin of the shear strain in the endomysium due to the contraction of the muscle fiber with the endomysial end attached to the muscle deforming while the remote end is fixed; this is consistent with a computational model that explored force transmission pathways (15). In this paper, the convention that the shear strain rate sign is positive when the shear angle is acute is followed (shear angle is shown in Fig. 1b). In addition to the fiber basis, the SR tensor in the principal axis frame is rotated by 45° to obtain the maximum shear strain (SR_{fc_max}).

ROI measurements—For each subject, the entire length of the MG was divided into three regions based on the distance from the most distal point of the muscle: bottom 25% (distal), mid-50% (middle), top 25% (proximal). Regional analysis of scalar indices derived from the SR tensor was performed on ROIs selected on the magnitude images in the three regions. Five to seven oblique-sagittal slices were acquired in each subject to cover the entire width of the MG; the average over all slices for each region is reported in the rest of the paper (an average over slices was used to increase the statistical power). For each slice, the size of the ROI was set at 7×7 voxels for the proximal and middle regions and at 5×10 for the distal region to accommodate the muscle taper. The ROI size was determined from empirical examinations of the biggest size ROI that could be placed within the region boundaries while avoiding the low intensity fat layers that ran along the fascicles. In order to ensure that the same anatomic region was reported, each pixel in the ROI was tracked (with respect to the first frame) to locate the new pixel positions in successive frames, creating a frame based ROI. Tracking was performed in 2D using the in-plane velocity information. The position in a subsequent frame was calculated based on the velocity information in the current frame. This allowed automated placement of an ROI in each frame that moved synchronously with the underlying anatomy (16). ROIs changed both location and shape (5 to 20% in successive frames) but the number of points was kept constant to ensure the average was based on the same number of points/frame. It is important to note that due to force losses consequent to the intervention, MR images were acquired at the same relative but lower absolute force levels post-suspension. To avoid bias related to different absolute force levels, average ROI values of the SR indices were extracted at the maximum force level subjects generated in the post-suspension state. The force recording was at much higher frequency than the MRI

temporal resolution; the force corresponding to each MR temporal frame was extracted with the assumption that 600 force points and 22 MR frames were uniformly spaced in the contraction cycle of 3 seconds.

Statistical analyses—The outcome variables of the analysis are the eigenvalues of the SR tensor (SR_{fiber}, $SR_{in\text{-}plane}$, $SR_{through\text{-}plane}$), the angle subtended by the principal axis of contraction and fiber direction (SR-fiber angle), the 2D SR components in the fiber basis (SR_{ff}, SR_{cc}, SR_{fc}) and the maximum shear strain, SR_{fc_max}. Prior to the analysis of significance, normality of data was tested using both the Shapiro-Wilk test and by visual inspection of Q-Q plots. The quantile-quantile (Q-Q) plot is an exploratory graphical device used to check the validity of a distributional assumption for a data set; in the current analysis it was tested for normality (Gaussian distribution). If the data can be represented by a normal distribution, then it is valid to employ parametric analysis such as ANOVA. Only moderate deviations from normality were found in several data groups, thus the difference between pre and post ULLS groups (termed time) and muscle regions as well as potential interaction effects (time*region) were accessed using repeated measures two-way analysis of variance (ANOVAs) (25–27). In case of significant ANOVA results for factor “region” post hoc paired-sample t-tests were done using Šidak’s correction of p-values. Data are reported as mean ± standard deviation (SD). For all tests, the level of significance was set at a $\alpha = 0.05$. The statistical analyses were carried out using SPSS for Mac OSX (SPSS 23.0, SPSS Inc., Chicago, IL).

Univariate and stepwise multivariate linear regression was performed to identify predictors (strain rate and morphological parameters of the Triceps Surae) of force and force change with disuse atrophy. In multivariate analysis, only independent variables were retained. For any two dependent variables, the one with the highest correlation (beta value) was retained in the multivariate analysis. Parameters excluded from the multivariable analysis were the SR in the fiber basis that significantly correlated with SR in principal axis basis and with SR_{fc_max} and ACSA, PCSA that significantly correlated with volume of the muscles.

Results

The average change (over all 7 subjects) in the volume of the MG, LG, and SOL muscles post-suspension are −9.6 ± 4.5 %, −11.1 ± 7.4 % and −7.4 ± 5.9 %, respectively while the average change in MVC is −32.6 ± 24.7 %; both force and morphological changes (volume and ACSA) are significant (Table 1). As reported in earlier studies, the force (MVC) loss is approximately 3 fold greater than the average volume loss and thus cannot be completely explained by muscle atrophy alone (change in muscle volume). Further, force normalized to cross-sectional area showed a reduction of 28.7 ± 24.6% post-suspension suggesting that changes in area (atrophy) cannot explain all of the loss in MVC for these muscles.

The main change visualized in the eigenvalue maps is the decrease in $SR_{in\text{-}plane}$ and increase in $SR_{through\text{-}plane}$ on unloading (Figure 2). Cine images of the streamlines representing the SR_{fiber} eigenvectors were generated for one subject (pre- suspension) (Supporting Video S1a and S1b); these streamlines are initiated on a coarse 4×4 pixel grid and track the negative

(Supporting Video S1a) and positive (Supporting Video S1b) eigenvectors as a function of the isometric cycle.

The temporal variation of the regional SR-fiber angles and though-plane SR eigenvalue with isometric contraction is shown in Figure 3 for pre- and post-suspension (to maintain continuity in the plot, the angle plot is the angle NEV makes with the muscle fiber) while the temporal variation in NEV and PEV is shown in Supporting Figure S1. The plots confirm the SR eigenvalue maps (Figure 3) in that the changes post-suspension are seen primarily in $SR_{in\text{-}plane}$ (in Supporting Figure S1, compare the second peak in NEV plot and first peak in PEV plot in pre- and post-suspension; these peaks correspond to $SR_{in\text{-}plane}$). Further, there is an increase in the SR-fiber angle post-suspension at the peak of the contraction phase. This increase in SR-fiber angle post-suspension is shown in Figure 4 for one subject in the zoomed portion of the MG where the fibers (fascicles manually tracked as solid black lines) are superposed on the SR streamlines. Figure 5 and Supporting Figure S1 are plots of the temporal variation of the strain rates in the fiber basis. As in the principal axes basis, the largest changes are seen in the deformation rate in the fiber cross-section (plot of SR_{cc} in Supporting Figure S1).

The values of the SR indices in the principal axes and in the fiber basis were extracted at the force value corresponding to the post-suspension value of each subject (a subject was compared between the pre- and post-suspension states at the (lower) force level of the post-suspension) (Table 2). $SR_{in\text{-}plane}$ in the pre-ULLS was significantly larger than in the post-ULLS cohort ($F(1,6) = 17.734$, $P = 0.006$). Significant difference in $SR_{in\text{-}plane}$ was also found between different muscle regions ($F(2,12)=12.090$, $P=0.001$). Follow up post hoc tests revealed that $SR_{in\text{-}plane}$ was larger in the distal compared to the proximal ($P=0.029$) and middle regions ($P=0.034$). SR-fiber angle was significantly larger post- ULLS ($F(1,6)=9.435$, $P=0.022$). Significant time (pre, post)*region (proximal, middle, distal) interaction effects were found for $SR_{through\text{-}plane}$ ($F(2, 12) = 8.484$, $P=0.005$). For the components of strain rate in fiber/cross-section basis, a trend to significance was observed between pre and post-suspension in SR_{cc} ($F(1,6) = 4.536$, $P=0.077$) which reflects the changes seen in $SR_{in\text{-}plane}$ in the principal axes basis. Though normal and shear strain rates (fiber basis or maximum) decreased in the post-suspension subjects (Table 2) no significant differences were detected. Significant regional differences were observed in the shear strain rate (SR_{fc}) ($F(2,12)=19.924$, $P=0.004$) with significantly larger shear strain rates in the distal ($P=0.013$) and middle ($P=0.009$) as compared to the proximal muscle region. Similar regional differences were seen in SR_{fc_max} ($F(2,12)=10.537$, $P=0.012$) with significantly larger shear strain rates in the distal ($P=0.041$) and middle ($P=0.023$) compared to the proximal region. No significant interactions effects of time (pre-post)*region (proximal, middle, distal) were found.

The results of the univariate/multivariate regression analysis for force and for force changes are summarized in Tables 3 and 4. For the univariate analysis, the absolute value of beta refers to the correlation coefficient for a given predictor and a significant p-value ($p<0.05$) associated with a predictor indicates that the null hypothesis that beta is zero for that variable is rejected. For multivariate analysis, the R value is the multiple correlation coefficient and is a measure of the quality of the prediction of force; the value of 0.844

(Table 3) indicates a good level of prediction. The beta values provide a relative weight of each predictor in the multivariate regression and a significant p-value ($p<0.05$) associated with a predictor indicates that the null hypothesis for that variable is rejected. Stepwise multivariate analysis selected $SR_{in\text{-}plane}$, SR-fiber angle and VOL_{MG} as significant predictors of force ($R=0.844$, $F=31.257$, $p<0.001$). Due to the small number of subjects for force change (7 subjects), the univariate analysis was not extended to multivariate analysis for prediction of force change. Univariate analysis identified the SR_{fiber} and maximum shear strain (SR_{fc_max}) as significantly associated with change in force with unloading (Table 4).

DISCUSSION AND CONCLUSION

In this study, an exploratory analysis of indices derived from the SR tensor was performed to determine any limb suspension related changes with the anticipation that these indices can be related to ECM remodeling. It is to be noted that all the SR analysis was conducted at the same force level for pre- and post-suspension (that corresponding to the post-suspension force) and hence it was not at the peak force for the pre-suspension data. However this insured that comparisons were not biased by different force levels for the pre- and post-suspension data. Further, a loss of ~30% (from the suspension intervention) shifted the point from peak force close to the beginning of the plateau level so that the pre-suspension values were not acquired too early in the contraction cycle. While not reported here, data was also analyzed at the peak force (corresponding to the peak in SR_{fiber} during the contraction phase of the isometric cycle) and showed the same trends and significant differences between pre- and post-intervention as analysis at the same force level. It should be noted that comparison at the peak force corresponds to analysis at the same %MVC in contrast to the same force. A detailed comparison of data analyzed at same force and at same %MVC (peak force) is the subject of an upcoming paper.

SR_{fiber} and SR_{ff} are the normal strain rate in a direction closest to the muscle fiber in the two basis. Though the two strain rates decreased post-suspension, the differences were not significant (Table 2). This is in contrast to findings in the aging study where younger cohorts showed significantly higher strain rates than older cohorts at isometric contraction (16). One of the hypotheses advanced to explain the age related decrease in strain rate was an increase in muscle stiffness with age arising from the remodeling of the extracellular matrix. Computational models predict that a stiffer extracellular matrix will result in reduced fascicle strain as well as force output (28). It is likely that the extensive ECM remodeling with the aging atrophy model that results in increased stiffness of the matrix is not present in the disuse atrophy model investigated herein or the increase in stiffness in ECM may not be as pronounced. However, there is increasing evidence that changes in the ECM play an important role in disuse-muscle atrophy. This is because disruption of muscle cell adhesion to the extracellular matrix leads to muscle wasting (29,30). For instance, degeneration of basal membrane components by matrix metalloproteases (MMPs) and alterations in mRNA and protein for extracellular matrix components have been found in disuse-muscle atrophy (29,30).

Significant decreases in $SR_{in\text{-}plane}$ are seen post-suspension (Table 2). The changes in $SR_{in\text{-}plane}$ reflect the changes in deformation asymmetry in the fiber cross-section. In

general, the reduction in $SR_{in\text{-}plane}$ indicates that asymmetry of deformation in the fiber cross-section is reduced post-suspension. While deformation asymmetry is most pronounced in the distal regions in both pre- and post-suspension, the axis of greater deformation changes from in-plane (pre) to through-plane (post) in the distal regions. Similar to $SR_{in\text{-}plane}$, SR_{cc} which is the in-plane deformation in the fiber basis, is reduced post-suspension with a trend to significance (Table 2). Asymmetry in deformation in the fiber cross-section has been reported in prior studies (16,31,32) and one hypothesis for asymmetric deformation is that constraints (to deformation) are introduced by a specific orientation of tensile material (e.g. costameres). Costameres can be described in simple terms as a protein assembly that anchors myofibrils to the sarcolemma and to the extracellular matrix, and thus acts as important bridge between the muscle's contractile and other structural components (33). Prior studies using the ULLS model identified a large decrease in costameric proteins, such as focal adhesion kinase, which could potentially contribute to the disproportionate loss of muscle force (30%) compared to the decrease in quadriceps muscle CSA (~5%) (8,17). This is because costameres provide the key functional role of adhesion between adjacent muscle fibers and between muscle fibers and the surrounding connective tissue (34). An earlier modeling paper predicted that when there is a strongly anisotropic constraint (which was postulated to arise from a specific structural arrangement of costameres), the force output may increase by a factor of two (28). Conversely, it is reasonable to speculate that when the anisotropy in stiffness decreases (implied by the decrease in asymmetry of deformation) it could account for the loss of force seen post-suspension.

Regional differences in $SR_{in\text{-}plane}$ eigenvalues were seen with distal regions showing the highest strain rates. Spatial heterogeneity of $SR_{in\text{-}plane}$ and $SR_{through\text{-}plane}$ is related to the regional variation of the asymmetry of deformation in the fiber cross section. The increasing deformation asymmetry at the distal end in the pre-suspension cohort may be related to the fiber packing density along the muscle length that increases from proximal to distal regions. Earlier studies have also reported regional heterogeneity in strain in the calf muscles (24) and in the brachis plexus (35). The reduced asymmetry even in distal regions for the post-suspension cohort (Table 2) could arise from a combination of fiber atrophy and from alterations in the ECM.

The deviation (non-zero SR-fiber angle, Table 2) of the principle axis of contraction from the muscle fiber orientation is seen in both pre- and post-suspension and this angle increases significantly post-suspension. Deviation of the principal axis of strain from that of the fiber has been observed in other muscles such as the anterior tibialis (31), biceps brachii (35) and the myocardium (36) and this deviation has been attributed to shearing between muscle fibers (37,38). The larger SR-fiber angle post-suspension may be related to an increase in SR_{fiber} heterogeneity (Table 2 shows that SR_{fiber} values in distal regions is higher by 50% compared to proximal regions in the post-suspension cohort; equivalent value in the pre-suspension data is 5%). It is likely that in the post-suspension state, the much higher relative strain rates in the distal regions results in larger SR-fiber angles through the shearing of the endomysium.

Shear strain rates (schematic shown in Fig. 1b) are related to SR-fiber angles and Eqn. 2 shows the relationship between the two variables (shear strain rate increases with the SR-fiber angle). However, it can be seen from Table 2 that shear strain rates (SR_{fc} and SR_{fc_max}) calculated from the eigenvalues and SR-fiber angle decrease in all three regions post-suspension. This decrease (in SR_{fc} *and* SR_{fc_max}) is essentially from the decrease in SR_{fiber} and in $SR_{in\text{-}plane}$ values post-suspension. Computational models predict that, in the prematurely terminating fiber, shearing of the endomysium is the most likely pathway for lateral transmission of force produced by the non-spanning fibers (15). The observed reduction in shear strain rate (in fiber basis or max shear strain basis) with suspension did not reach significance but it may be speculated that the changes in SR_{fc}/SR_{fc_max} may translate to a reduction in lateral transmission of force. This reduction in LTF may then account for the loss in total force that is not explained by muscle atrophy, activation, and specific tension changes with unloading.

The identification of $SR_{in\text{-}plane}$, SR-fiber angle and VOL_{MG} in stepwise multivariate regression as significant predictors of force has interesting physiological implications. The volume of the MG muscle may reflect the size and number of muscle fibers as well as the extent of connective tissue as well as fatty infiltration. While aging has been shown to lead to increase in fatty infiltration as well as an increase in the width of connective tissue (39), preliminary results on suspension induced disuse atrophy from our group did not reveal a change in fat or connective tissue content. Thus, it is plausible to infer that volume differences in the MG within the cohort of pre- and post- suspension subjects reflect the size and number of muscle fibers and since the size/number of muscle fibers determines contractility, it is anticipated to be a predictor of force. R10 The relationship of $SR_{in\text{-}plane}$ and SR-fiber angle to force is more complex: $SR_{in\text{-}plane}$ reflects the constraints (in the extracellular matrix) that modulate the extent of deformation in-plane that, as detailed earlier, may have an effect on the total force produced. SR-fiber angle is related to shear in the endomysium (Fig. 1). Since $SR_{in\text{-}plane}$ and SR-fiber angle are parameters that are influenced by the ECM, their relationship to force highlights the role of the ECM in the force output. In univariate analysis, the significant predictors of force change with unloading are the SR eigenvalues and SR_{fc_max}. SR_{fiber} is a measure of contractility in the fiber direction and a decrease in its magnitude is anticipated to correlate to force loss. $SR_{in\text{-}plane}$ and $SR_{through\text{-}plane}$ reflect the deformation asymmetry in the fiber cross-section and are influenced by changes in the ECM. SR_{fc_max}, the shear strain rate is also influenced by ECM remodeling and further, is postulated as the mechanism of lateral transmission of force; a decrease in the shear strain rate may potentially reduce lateral transmission of force (LTF). While changes in the ECM with unloading have been reported in prior studies (13) and it has been postulated that this remodeling may result in modulating the lateral force transmission pathway leading to a loss of force output (14), this is the first study to show that force changes (*in vivo* and in human subjects) on uploading are related to changes in shear strain. It should be noted that there are other determinants that will also contribute to force loss with unloading but in this exploratory work on a small cohort, the intent was to extract the contributions of the strain rates in the MG and morphological parameters of the plantarflexors to changes in force production.

The limitations of this study are as follows. The number of subjects is small; however this was still sufficient to find significant differences in some of the SR indices during isometric contraction between the pre- and post-suspension cohorts and to detect significant regional differences. Muscle fiber and its direction were indirectly determined and the accuracy of the fiber orientation depends on the accuracy of locating fascicles in the magnitude images. On the other hand, diffusion tensor imaging provides fiber directions directly. However, it should be noted that the method used in the current paper is the only way to track muscle fibers over a large region of interest through the dynamic cycle. Finally, noise in the imaging data can cause error propagation in the calculated indices especially as the computation involves the gradients of images that cause noise to be amplified.

The paper confirms the overarching hypothesis that some of the indices derived from the strain rate tensor (SR) will show significant changes after unloading and that force loss in disuse atrophy will be predicted by SR parameters that are known to be influenced by the ECM remodeling. The two indices that showed significant changes were $SR_{in\text{-}plane}$ and the SR-fiber angle; both these parameters are influenced by the ECM. Further, $SR_{in\text{-}plane}$, SR-fiber angle, and VOL_{MG} were identified from a multivariable regression analysis as predictors of force. SR_{fiber}, $SR_{in\text{-}plane}$, $SR_{through\text{-}plane}$, SR_{fc_max} were significant predictors of force change in univariate analysis. SR_{fc_max} reflects changes in ECM and importantly, the study shows that the shear strain rate (and potentially lateral transmission of force) is a predictor of force loss with atrophy. The role of the ECM (and remodeling) is increasingly being identified in several musculoskeletal diseases states including muscular dystrophies, diabetes, and aging (40). Lateral transmission of force may be impacted by changes in the ECM and techniques to non-invasively monitor ECM remodeling and its functional consequence may allow accurate diagnosis and tracking of these disease states, ability to tailor rehabilitative paradigms and to monitor the efficacy of drug interventions.

Supplementary Material

Refer to Web version on PubMed Central for supplementary material.

References

1. Bodine SC. Disuse-induced muscle wasting. Int J Biochem Cell Biol. 2013; 45(10):2200–2208. [PubMed: 23800384]
2. Bongers KS, Fox DK, Kunkel SD, Stebounova LV, Murry DJ, Pufall MA, Ebert SM, Dyle MC, Bullard SA, Dierdorff JM, Adams CM. Spermine oxidase maintains basal skeletal muscle gene expression and fiber size and is strongly repressed by conditions that cause skeletal muscle atrophy. Am J Physiol Endocrinol Metab. 2015; 308(2):E144–158. [PubMed: 25406264]
3. Thomason DB, Booth FW. Atrophy of the soleus muscle by hindlimb unweighting. J Appl Physiol (1985). 1990; 68(1):1–12. [PubMed: 2179205]
4. Narici M, Cerretelli P. Changes in human muscle architecture in disuse-atrophy evaluated by ultrasound imaging. J Gravit Physiol. 1998; 5(1):P73–74. [PubMed: 11542371]
5. Seynnes OR, Maganaris CN, de Boer MD, di Prampero PE, Narici MV. Early structural adaptations to unloading in the human calf muscles. Acta Physiol (Oxf). 2008; 193(3):265–274. [PubMed: 18266998]
6. Li R, Narici MV, Erskine RM, Seynnes OR, Rittweger J, Pisot R, Simunic B, Fluck M. Costamere remodeling with muscle loading and unloading in healthy young men. J Anat. 2013; 223(5):525–536. [PubMed: 24010829]

7. Narici M, Franchi M, Maganaris C. Muscle structural assembly and functional consequences. J Exp Biol. 2016; 219(Pt 2):276–284. [PubMed: 26792340]
8. de Boer MD, Maganaris CN, Seynnes OR, Rennie MJ, Narici MV. Time course of muscular, neural and tendinous adaptations to 23 day unilateral lower-limb suspension in young men. J Physiol. 2007; 583(Pt 3):1079–1091. [PubMed: 17656438]
9. D'Antona G, Pellegrino MA, Adami R, Rossi R, Carlizzi CN, Canepari M, Saltin B, Bottinelli R. The effect of ageing and immobilization on structure and function of human skeletal muscle fibres. J Physiol. 2003; 552(Pt 2):499–511. [PubMed: 14561832]
10. Trappe S, Trappe T, Gallagher P, Harber M, Alkner B, Tesch P. Human single muscle fibre function with 84 day bed-rest and resistance exercise. J Physiol. 2004; 557(Pt 2):501–513. [PubMed: 15064323]
11. Zhang C, Gao Y. Effects of aging on the lateral transmission of force in rat skeletal muscle. J Biomech. 2014; 47(5):944–948. [PubMed: 24507947]
12. Street SF. Lateral transmission of tension in frog myofibers: a myofibrillar network and transverse cytoskeletal connections are possible transmitters. J Cell Physiol. 1983; 114(3):346–364. [PubMed: 6601109]
13. Lieber RL, Ward SR. Cellular mechanisms of tissue fibrosis. 4. Structural and functional consequences of skeletal muscle fibrosis. Am J Physiol Cell Physiol. 2013; 305(3):C241–252. [PubMed: 23761627]
14. Ramaswamy KS, Palmer ML, van der Meulen JH, Renoux A, Kostrominova TY, Michele DE, Faulkner JA. Lateral transmission of force is impaired in skeletal muscles of dystrophic mice and very old rats. J Physiol-London. 2011; 589(5):1195–1208. [PubMed: 21224224]
15. Sharafi B, Blemker SS. A mathematical model of force transmission from intrafascicularly terminating muscle fibers. J Biomech. 2011; 44(11):2031–2039. [PubMed: 21676398]
16. Sinha U, Malis V, Csapo R, Moghadasi A, Kinugasa R, Sinha S. Age-Related Differences in Strain Rate Tensor of the Medial Gastrocnemius Muscle During Passive Plantarflexion and Active Isometric Contraction Using Velocity Encoded MR Imaging: Potential Index of Lateral Force Transmission. Magn Reson Med. 2015; 73(5):1852–1863. [PubMed: 25046255]
17. Brocca L, Longa E, Cannavino J, Seynnes O, de Vito G, McPhee J, Narici M, Pellegrino MA, Bottinelli R. Human skeletal muscle fibre contractile properties and proteomic profile: adaptations to 3 weeks of unilateral lower limb suspension and active recovery. J Physiol. 2015; 593(24):5361–5385. [PubMed: 26369674]
18. de Boer MD, Selby A, Atherton P, Smith K, Seynnes OR, Maganaris CN, Maffulli N, Movin T, Narici MV, Rennie MJ. The temporal responses of protein synthesis, gene expression and cell signalling in human quadriceps muscle and patellar tendon to disuse. J Physiol-London. 2007; 585(1):241–251. [PubMed: 17901116]
19. Horstman AM, de Ruiter CJ, van Duijnhoven NT, Hopman MT, de Haan A. Changes in muscle contractile characteristics and jump height following 24 days of unilateral lower limb suspension. Eur J Appl Physiol. 2012; 112(1):135–144. [PubMed: 21505844]
20. Clarke EC, Martin JH, d'Entremont AG, Pandy MG, Wilson DR, Herbert RD. A non-invasive, 3D, dynamic MRI method for measuring muscle moment arms in vivo: demonstration in the human ankle joint and Achilles tendon. Med Eng Phys. 2015; 37(1):93–99. [PubMed: 25466777]
21. Csapo R, Malis V, Hodgson J, Sinha S. Age-related greater Achilles tendon compliance is not associated with larger plantar flexor muscle fascicle strains in senior women. J Appl Physiol. 2014; 116(8):961–969. [PubMed: 24505104]
22. Gindre J, Takaza M, Moerman KM, Simms CK. A structural model of passive skeletal muscle shows two reinforcement processes in resisting deformation. J Mech Behav Biomed Mater. 2013; 22:84–94. [PubMed: 23587721]
23. Kim H, Yoo L, Shin A, Demer JL. Determination of poisson ratio of bovine extraocular muscle by computed X-ray tomography. Biomed Res Int. 2013; 2013:197479. [PubMed: 23484091]
24. Shin DD, Hodgson JA, Edgerton VR, Sinha S. In vivo intramuscular fascicle-aponeuroses dynamics of the human medial gastrocnemius during plantarflexion and dorsiflexion of the foot. J Appl Physiol. 2009; 107(4):1276–1284. [PubMed: 19608924]
25. Harwell MR. Summarizing Monte Carlo Results in Methodological Research. 1992:297–313.

26. Glass GV, Peckham PD, Sanders JR. Consequences of Failure to Meet Assumptions Underlying the Fixed Effects Analyses of Variance and Covariance. 1972
27. Lix LM, Keselman JC, Keselman HJ. Consequences of Assumption Violations Revisited: A Quantitative Review of Alternatives to the One-Way Analysis of Variance "F" Test. Review of Educational Research. 1996; 66(4):579–619.
28. Hodgson JA, Chi SW, Yang JP, Chen JS, Edgerton VR, Sinha S. Finite element modeling of passive material influence on the deformation and force output of skeletal muscle. J Mech Behav Biomed. 2012; 9:163–183.
29. Giannelli G, De Marzo A, Marinosci F, Antonaci S. Matrix metalloproteinase imbalance in muscle disuse atrophy. Histol Histopathol. 2005; 20(1):99–106. [PubMed: 15578428]
30. Urso ML, Scrimgeour AG, Chen YW, Thompson PD, Clarkson PM. Analysis of human skeletal muscle after 48 h immobilization reveals alterations in mRNA and protein for extracellular matrix components. J Appl Physiol (1985). 2006; 101(4):1136–1148. [PubMed: 16763108]
31. Englund EK, Elder CP, Xu Q, Ding Z, Damon BM. Combined diffusion and strain tensor MRI reveals a heterogeneous, planar pattern of strain development during isometric muscle contraction. Am J Physiol Regul Integr Comp Physiol. 2011; 300(5):R1079–1090. [PubMed: 21270344]
32. van Donkelaar CC, Willems PJ, Muijtjens AM, Drost MR. Skeletal muscle transverse strain during isometric contraction at different lengths. J Biomech. 1999; 32(8):755–762. [PubMed: 10433416]
33. Bloch RJ, Capetanaki Y, O'Neill A, Reed P, Williams MW, Resneck WG, Porter NC, Ursitti JA. Costameres: repeating structures at the sarcolemma of skeletal muscle. Clin Orthop Relat Res. 2002; (403 Suppl):S203–210. [PubMed: 12394470]
34. Gullberg D, Velling T, Lohikangas L, Tiger CF. Integrins during muscle development and in muscular dystrophies. Front Biosci. 1998; 3:D1039–1050. [PubMed: 9778539]
35. Zhong X, Epstein FH, Spottiswoode BS, Helm PA, Blemker SS. Imaging two-dimensional displacements and strains in skeletal muscle during joint motion by cine DENSE MR. J Biomech. 2008; 41(3):532–540. [PubMed: 18177655]
36. Pilla JJ, Koomalsingh KJ, McGarvey JR, Witschey WR, Dougherty L, Gorman JH 3rd, Gorman RC. Regional myocardial three-dimensional principal strains during postinfarction remodeling. Ann Thorac Surg. 2015; 99(3):770–778. [PubMed: 25620591]
37. Huijing PA. Muscle as a collagen fiber reinforced composite: a review of force transmission in muscle and whole limb. Journal of Biomechanics. 1999; 32(4):329–345. [PubMed: 10213024]
38. Purslow PP. The structure and functional significance of variations in the connective tissue within muscle. Comp Biochem Phys A. 2002; 133(4):947–966.
39. Csapo R, Malis V, Sinha U, Du J, Sinha S. Age-associated differences in triceps surae muscle composition and strength - an MRI-based cross-sectional comparison of contractile, adipose and connective tissue. BMC Musculoskelet Disord. 2014; 15:209. [PubMed: 24939372]
40. Gillies AR, Lieber RL. Structure and function of the skeletal muscle extracellular matrix. Muscle Nerve. 2011; 44:318–331. [PubMed: 21949456]

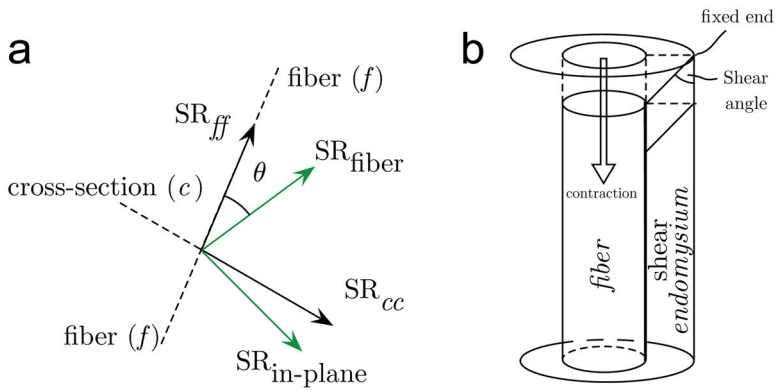

Figure 1.

The relative orientation of the 2D principal axes of strain rate (SR_{fiber}, $SR_{in\text{-}plane}$) compared to that of the muscle fiber (normal strain along the fiber is denoted as SR_{ff}) and cross-section (normal strain in the fiber cross section is denoted as SR_{cc}) in isometric (1a). Shear strain is the off-diagonal term obtained by rotating the tensor from the principal basis to that of the muscle fiber basis and its origin is schematically shown in 1b (muscle and endomysium not drawn to scale). In the current shear strain model one end of the endomysium is fixed while the other end moves with the muscle fiber (muscle fiber contracts); the dotted outline is that of the undeformed element in the endomysium and the solid line is the deformed element due to muscle contraction (1b).

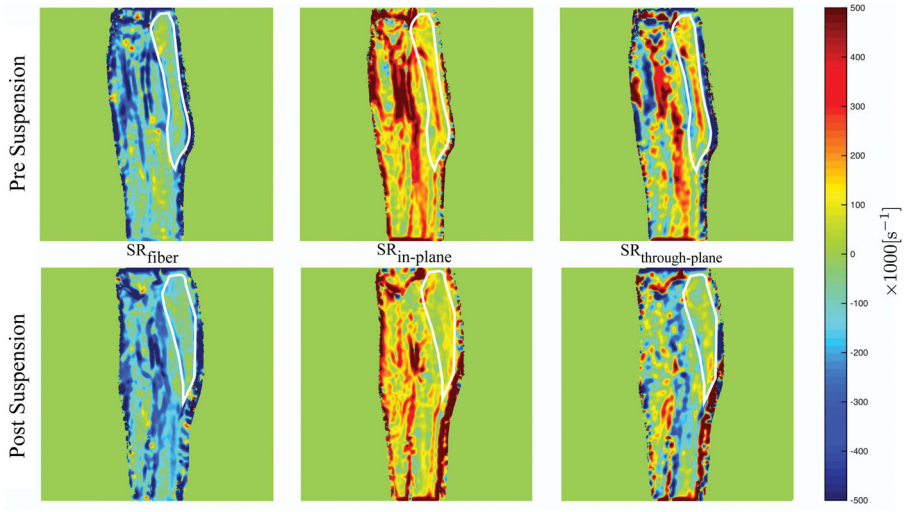

Figure 2.

Eigenvalue colormaps corresponding to one subject at baseline (Pre-suspension) and immediately after the 4 week of unloading (Post-suspension) during isometric contraction at the peak of the contraction phase. Visually, a decrease in $SR_{in\text{-}plane}$ and an increase in $SR_{through\text{-}plane}$ is seen in the post-suspension images compared to the pre-suspension images. The MG is outlined in white for ease of visualization.

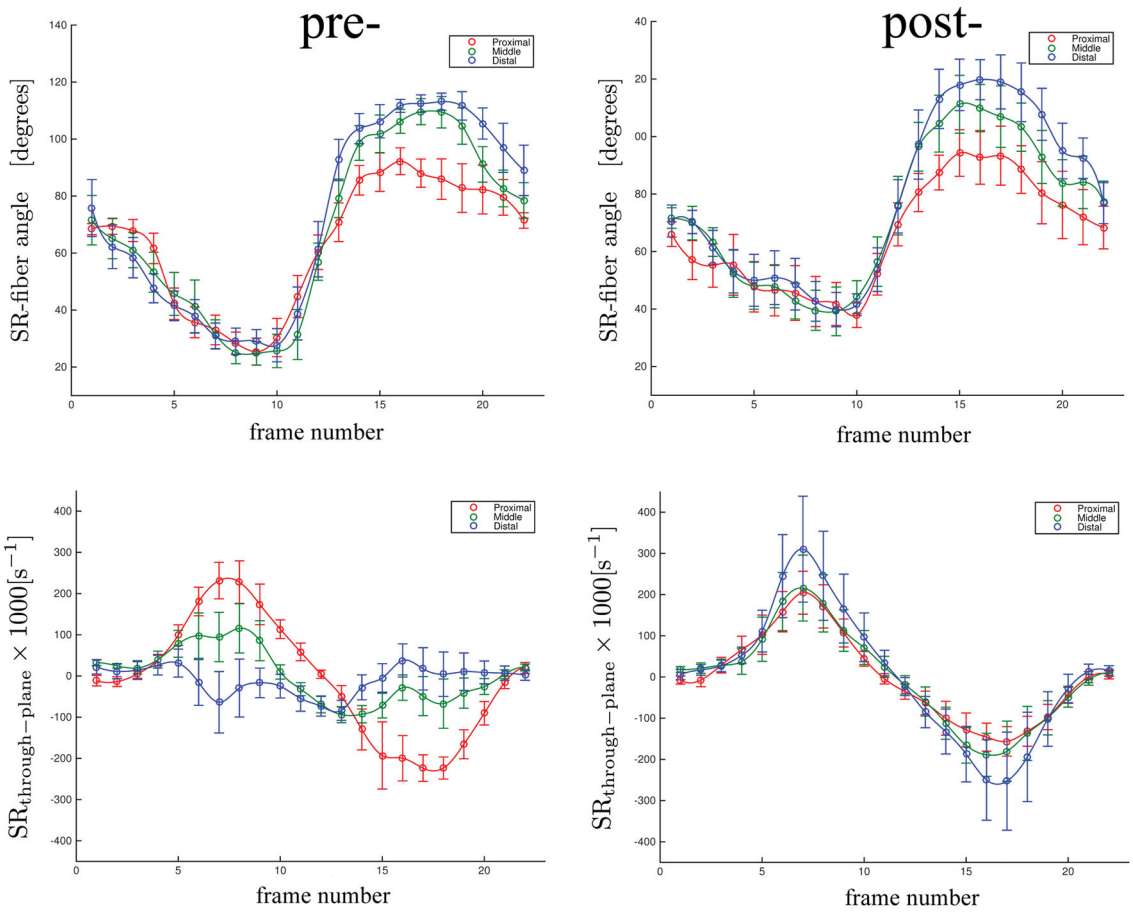

Figure 3.

The temporal variation of the SR-fiber angle and $SR_{through\text{-}plane}$ with isometric contraction for the pre- and post-suspension cohorts for three regions (proximal, middle, and distal). The values shown in this plot are the average over all subjects of all 7 slices for 3 ROIs (proximal, middle and distal) for the pre-and post-suspension subjects. The jump in the temporal plots of the SR-fiber angle occurs when the negative SR eigenvector direction changes abruptly as the cycle switches to relaxation (from contraction) at phase 11. The SR values are scaled by 1000.

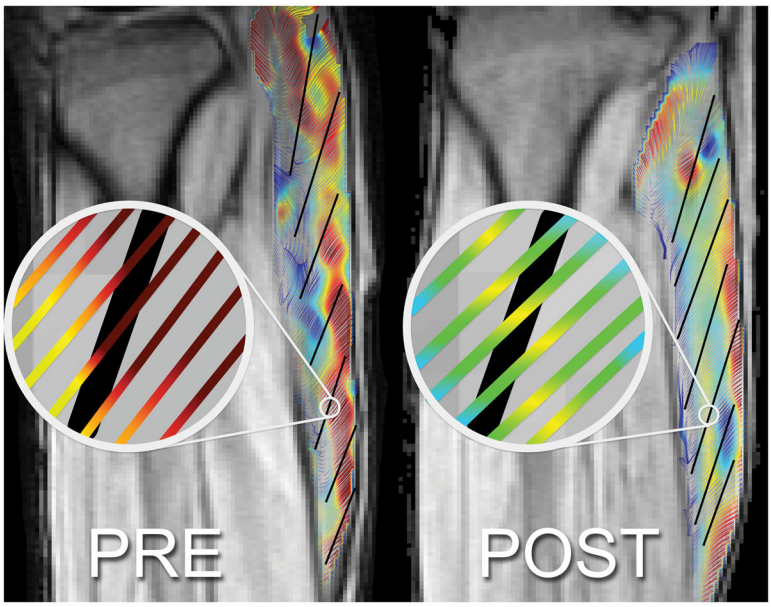

Figure 4.

Streamlines of eigenvectors corresponding to negative eigenvalues overlaid on fiber directions (in black tracked from fascicle orientations) for one slice of the same subject pre- and post-suspension during the contraction phase in the frame corresponding to max value of SR_{fiber}. This shows the difference in angle enclosed by SR_{fiber} and muscle fiber (SR-fiber angle).

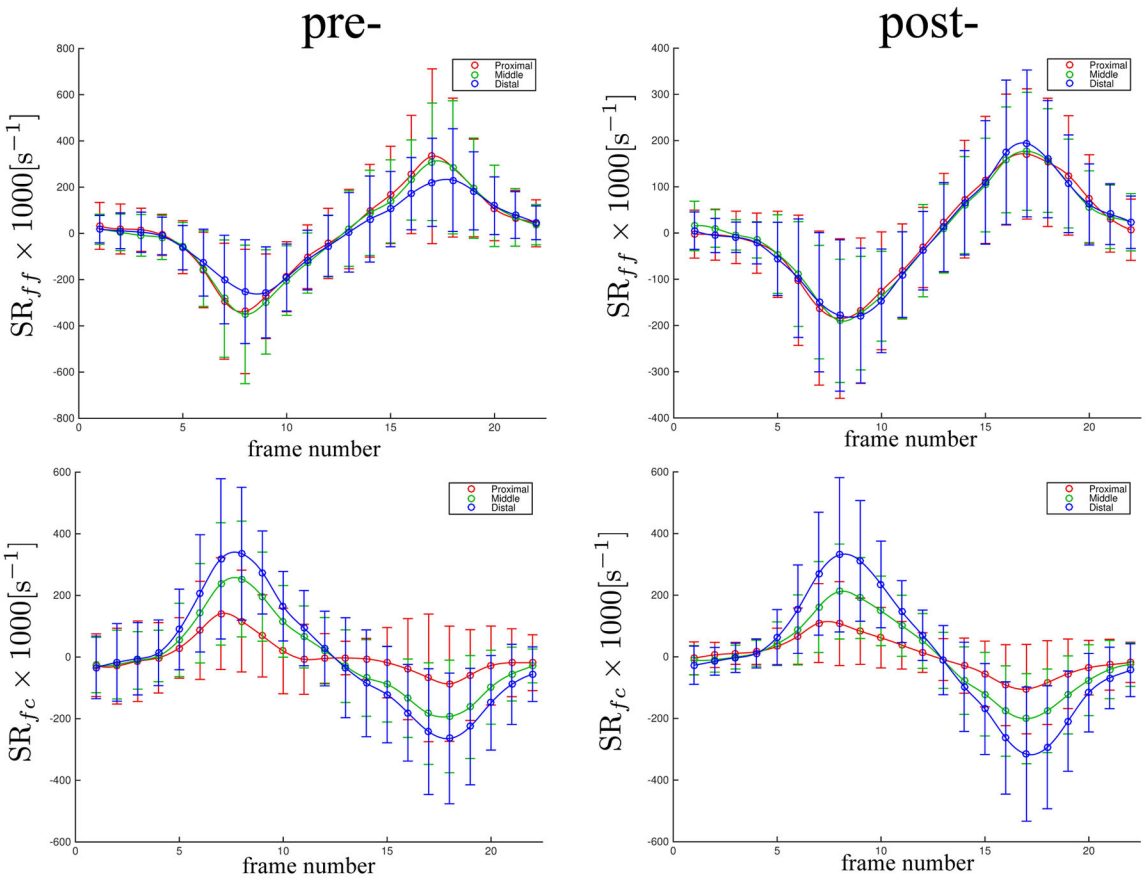

Figure 5.

The temporal variation of the SR values (normal strain rate: SR_{ff}, and shear strain rate: SR_{fc}) in the muscle fiber basis with isometric contractions for the pre- and post-suspension cohorts in three regions (proximal, middle and distal). The values shown in this plot are the average over all subjects of all 7 slices for the pre-and post-suspension subjects. The subscripts for the strain rate tensor, SR are: *ff* refers to the fiber axis, and *fc* refers to the shear term. The SR values are scaled by 1000.

Table 1

Force (Maximum Voluntary Contraction, MVC) and morphological parameters (Volume (VOL), Anatomical Cross-Sectional Area (ACSA) and Physiological Cross-Sectional Area (PCSA)) for individual muscles (Medial Gastrocnemius (MG), Lateral Gastrocnemius (LG), and Soleus (SOL)) of the plantarflexors.

	Pre-	Post-	P value
MVC[1] [N]	339.4 ± 91.5	225.6 ± 113.1	0.013
VOL_{MG1} [cm^3]	190.1 ± 69.2	172.3 ± 64.7	0.001
VOL_{LG1} [cm^3]	103.5 ± 45.3	91.4 ± 40.3	0.008
VOL_{SOL1} [cm^3]	448.2 ± 171.4	420.4 ± 177.9	0.006
$ACSA_{MG1}$ [cm^2]	15.4 ± 6.1	14.2 ± 6.1	0.005
$ACSA_{LG1}$ [cm^2]	9.4 ± 4.9	8.4 ± 4.3	0.020
$ACSA_{SOL}$ [cm^2]	25.4 ± 9.7	24.8 ± 10.6	0.291
$PCSA_{MG}$ [cm^2]	74.4 ± 21.5	57.1 ± 15.3	0.327

[1] significant difference between pre and post suspension

Table 2

Strain Rate tensor components in the principal axis basis, in the muscle fiber basis and in the maximum shear strain basis for pre- and post-suspension computed at the same force level in the contraction phase of the isometric contraction.

Isometric same force level	time	region		
		proximal	middle	distal
SR_{fiber} [×1000 s^{-1}]	pre	−448.48 ± 219.93	−478.67 ± 228.88	−496.81 ± 212.96
	post	−218.70 ± 138.91	−295.21 ± 223.73	−423.47 ± 362.89
$SR_{in\text{-}plane}$ [1,2,3] [×1000 s^{-1}]	pre	259.11 ± 79.04	377.76 ± 114.69	492.04 ± 249.22
	post	120.36 ± 77.36	161.17 ± 88.21	177.66 ± 63.40
$SR_{out\text{-}plane}$ [4] [×1000 s^{-1}]	pre	189.37 ± 201.99	100.91 ± 199.69	4.77 ± 205.97
	post	98.34 ± 180.06	134.03 ± 245.76	245.81 ± 359.86
SR-fiber angle [1] [degrees]	pre	27.09 ± 5.67	27.14 ± 7.93	32.45 ± 8.85
	post	45.3 ± 18.19	39.37 ± 15.78	44.58 ± 13.37
SR_{ff} [×1000 s^{-1}]	pre	−287.19 ± 207.43	−304.56 ± 214.32	−234.99 ± 81.65
	post	−132.67 ± 104.11	−155.42 ± 93.40	−166.9 ± 145.68
SR_{cc} [×1000 s^{-1}]	pre	112.56 ± 86.14	184.14 ± 134.39	192.76 ± 187.55
	post	−0.39 ± 147.18	5.51 ± 274.19	−156.89 ± 299.33
SR_{fc} [2,5] [×1000 s^{-1}]	pre	148.81 ± 145.57	229.88 ± 206.9	294.36 ± 237.35
	post	93.34 ± 60.97	187.99 ± 126.94	287.92 ± 198.53
SR_{fc_max} [2,5] [×1000 s^{-1}]	pre	295.75 ± 181.69	389.03 ± 229.29	409.13 ± 249.11
	post	198.38 ± 80.26	257.19 ± 112.06	369.34 ± 188.3

[1] significant difference between pre and post suspension

[2] significant difference between proximal and distal region

[3] significant difference between middle and distal region

[4] significant interaction time*region

[5] significant difference between proximal and middle region

Table 3

Univariate and multivariate linear regression analysis of morphological and strain rate parameters to the force output (Maximum Voluntary Contraction). Pre- and post- data were pooled together for the analysis.

	Univariate		Multivariate	
	Beta	**P value**	**Beta**	**P value**
SR_{fiber}	−0.124	0.433		
$SR_{in\text{-}plane}$	0.426	0.005	0.277	0.007
$SR_{out\text{-}plane}$	−0.129	0.222		
SR-fiber angle	−0.528	<0.001	−0.299	0.004
SR_{fc_max}	0.098	0.537		
VOL_{GM}	0.692	<0.001	.629	<0.001
VOL_{GL}	0.690	<0.001		
VOL_{SOL}	0.655	<0.001		

Table 4

Univariate linear regression analysis of changes in morphological and strain rate parameters to the change in force output (MVC) after unloading.

	Univariate	
	Beta	**P value**
SR_{fiber}	−0.732	< 0.001
$SR_{in\text{-}plane}$	0.468	0.032
$SR_{out\text{-}plane}$	0.582	0.006
SR-fiber angle	−0.242	0.290
SR_{fc_max}	0.721	<0.001
VOL_{GM}	0.286	0.217
VOL_{GL}	0.095	0.578
VOL_{SOL}	0.384	0.085